Synchrotron photoemission studies of the Sb-passivated Si surfaces: Degenerate doping and bulk band dispersions

D. H. Rich,* G. E. Franklin, F. M. Leibsle, T. Miller, and T.-C. Chiang
Department of Physics, University of Illinois at Urbana-Champaign, 1110 West Green Street, Urbana, Illinois 61801
and Materials Research Laboratory, University of Illinois at Urbana-Champaign, 104 South Goodwin Avenue, Urbana, Illinois 61801
(Received 21 August 1989)

Synchrotron photoemission of the Sb-covered Si(001), Si(111), and Si(110) surfaces revealed that the Fermi-level position crosses the conduction-band minimum (CBM) of Si for Sb coverages approaching a one-monolayer saturation limit. Momentum-resolved photoemission of the Sb-saturated Si(001) and Si(110) surfaces showed the existence of an occupied initial state located near the CBM. The photoemission intensity of the state has been examined as a function of photon energy with constant initial-state difference spectroscopy which showed various resonances occurring due to transitions to different final states from the CBM. The metallic character of the surface is shown to be due to degenerate doping in the near-surface region. Core-level spectroscopy of Sb/Si(111) and Sb/Si(001) revealed that the Si atoms in the near-surface region are converted to exhibit a bulklike arrangement after Sb coverage. The Sb saturation of Si(111) and Si(001) was found to allow the measurement of the bulk band-dispersion relations along the high-symmetry Γ-Λ-L and Γ-Δ-X directions over a wide photon-energy range (37–153 eV). Strain-reduction mechanisms in the near-surface region are discussed. The measured CBM-state resonances and the Si(001) bulk band transitions indicate that the effective mass of the free-electron-like final band changes for varying photon energies.

I. INTRODUCTION

The modification of the electronic structure of clean Si and Ge surfaces through adsorption of various materials has been a prevalent topic in surface studies over recent years. The propensity in industry towards a miniaturization of devices and fabrication of devices relying on novel forms of constructions requires constant improvements in knowledge regarding the electronic and structural phenomena which describe heterostructures. In particular, an optimization of diode devices which are based on negative resistance and tunneling principles for special low-power microwave and charge-coupled applications will require a knowledge of the factors controlling dopant incorporation in semiconductors, and thus, the degenerate doping of semiconductor surfaces and fabrication of δ-function doped interfaces are topics of high current interest. The ability to tailor surfaces or interfaces with sharp doping characteristics is extremely important, and molecular-beam-epitaxy- (MBE) prepared δ-function doping layers which exhibit quantum confinement of charge have been previously studied.[1,2]

In this paper we present the results of a synchrotron photoemission study of the Sb-terminated Si(001), Si(111), and Si(110) surfaces. For all three surfaces, the Fermi level is found to move just above the conduction-band minimum (CBM) of Si, resulting in a degenerate doping condition in the near-surface region. For Si(001) and Si(110), a distinct emission is measured within a narrow energy window defined by the CBM of Si. The angle-resolved photoemission techniques of "$k_\perp$ and $k_\parallel$ scans" are employed to measure the CBM positions in k space for the Si(001) surface. A previous study has examined the CBM-state resonance over a limited range in k space.[3] The resonance behavior is further examined here over a wider energy range and with a new variation of an old technique: constant-initial-state spectroscopy (CIS). The CIS technique was first employed by Lapeyre *et al.* for a measurement of the density of final states of KCl using an angle-integrated geometry.[4] In the present experiment the cross section of the CBM state is measured as a function of the photon energy by a differencing of emissions between two closely spaced initial-state positions to account for background emission, and we refer to this procedure as constant-initial-state–difference spectroscopy (CIDS). The photoemission measurements for Sb/Si(001) show three distinct CBM-state intensity resonances for varying photon energies, and are found to correlate well with the conduction-band structure of Si. A full determination of the wave vector k for the conduction-band minimum of Si is carried out. This work demonstrates that the Sb termination prepared by conventional MBE techniques can degenerately dope (n^{2+} type) the near-surface region of Si.

In addition, we apply the $k_\perp$-scan technique to measure the Si bulk valence-band structure along the [001] (Γ-Δ-X) and [111] (Γ-Λ-L) high-symmetry directions. The photoemission technique has proven to be a valuable tool for mapping the bulk band structure of important semiconductors such as GaAs and Ge.[5–8] Previous attempts

at obtaining the bulk band dispersions of Si by photoemission from the clean Si(111)-(7×7) and Si(001)-(2×1) surfaces have produced only very limited success. Using the normal-emission method, bulk band transitions from the valence bands to the free-electron-like final band were observed over a small part of the band structure for Si(001)-(2×1), while no measurable dispersion was seen for Si(111)-(7×7).[8] In a preliminary study, we have demonstrated that the Sb passivation of the Si(111) and Si(001) surfaces have facilitated the measurement of the Si bulk valence-band dispersion relations.[9] In this study we extend the measurements to a wider energy range to obtain a more complete valence-band dispersion relation. From the measured CBM-state resonance and the bulk band transitions, we have found it necessary to introduce an energy-dependent effective mass for the free-electron-like final band.

Core-level spectroscopy is used to examine the modification of the local chemical environment of the Si(111) and Si(001) surfaces by the Sb adsorption. From the core-level and bulk valence-band dispersion results, conclusions are drawn regarding a Sb-induced modification in strain occurring in the near-surface region of the Sb-terminated Si surfaces.

II. EXPERIMENTAL DETAILS

The photoemission experiments were carried out using synchrotron radiation from the University of Illinois beam line of Aladdin, the 1-GeV storage ring at the Synchroton Radiation Center of the University of Wisconsin—Madison at Stoughton, WI. Light from the ring was dispersed by a 6-m toroidal-grating monochromator and an extended-range grating monochromator,[10] which were used for the angle-resolved and angle-integrated photoemission measurements, respectively. A hemispherical analyzer having a full acceptance angle of 3° was employed for the angle-resolved normal-emission experiments, while an angle-integrating hemispherical analyzer was used for core-level measurements. The overall instrumental resolution was typically 100–200 meV. The sample Fermi level was determined by observing emission from the Fermi edge of a polycrystalline Au sample in electrical constant with the Si samples.

High-energy electron diffraction (HEED) was employed to assess the clean-surface reconstructions and changes due to the Sb termination; HEED and MBE were performed in the same vacuum chamber used for the photoemission measurements. The n-type Si(111) samples were cleaned by thermal treatment at 1250 °C, while the n-type Si(001) and Si(110) samples were both treated at 1100 °C. The reconstructions for clean Si(111), Si(001),and Si(110) were determined by HEED, which showed sharp (7×7), (2×1), and (4×5) patterns, respectively. The Sb overlayers were prepared by evaporation with a rate of 1–10 monolayers (ML) per minute. In this paper 1 ML of Sb is defined as the site density for the unreconstructed surface in question, which is 6.8×10^{14}, 7.8×10^{14}, and 9.6×10^{14} atoms/cm^2 for Si(001), Si(111), and Si(110), respectively. The sample temperature during evaporation was maintained within 320–370 °C. Upon exposure to the Sb beam, the sticking coefficient was found to approach zero once the surface coverage approached the saturation limit of approximately 1 ML,[11–13] and typical exposures of 30–50 ML were employed to ensure that full saturation was attained when desired. The HEED results indicated that the Sb/Si(111) system was transformed into a (1×1) surface at saturation, while the Sb/Si(001) system exhibited a very faint (2×1) ordering within a (1×1) pattern. The Sb/Si(110) system showed a sharp (2×3) pattern. The samples were allowed to cool to near room temperature before the photoemission measurements.

The CIDS technique used here is as follows. In the conventional CIS technique, the analyzer kinetic-energy passband and the monochromator are simultaneously scanned so that the difference between the photon energy $h\nu$ and kinetic energy E_k of the photoelectron remains constant (thus, the initial-state binding energy remains constant). The resulting intensity variation mainly reflects the density of the allowed final states for the given initial state. However, background emission at the initial-state binding energy is also included in the measurement. In CIDS, two CIS spectra are simultaneously acquired with the analyzer passband setting alternately switched back and forth for two initial states, one for the state of interest (the CBM state) and the other for a state nearby representing background emission. The differencing between the two spectra eliminates most of the background contribution. For the CBM-state intensity-resonance measurement, the reference initial state for background subtraction is chosen to be within the Si band gap; the emission is small yet measurable due to secondary excitations by the stray higher-order light from the monochromator.

III. RESULTS AND DISCUSSION

A. Si 2p and Sb 4d core levels for Si(001) and Si(111)

The Si 2p core-level spectra (dots) are shown in Fig. 1 for both the clean and Sb-saturated surfaces. Previous studies of the clean surfaces employing a nonlinear least-squares-fitting procedure have shown that the line shapes contain surface and bulk contributions; the details of this analysis can be found in earlier publications.[14–16] The Si(111)-(7×7) spectrum shows two surface components (labeled $S1$ and $S2$) in addition to the bulk component (labeled B), while the spectrum for the Si(001)-(2×1) surface shows one surface component (labeled S). These surface-shifted components have been related to specific details of the reconstruction.[14,16] For Sb coverages approaching saturation, the surface shifts become suppressed, and the core-level spectra in Fig. 1 are seen to convert to exhibit a single bulklike component. The simplest interpretation is that the adsorption of Sb causes all dangling bonds on the Si surfaces to become saturated and results in a bulklike fourfold bonding arrangement for the Si surface atoms. The surface-electronic topography of Sb/Si(100) has been examined with scanning tunneling microscopy (STM), which confirms the saturation of the dangling bonds.[13] This behavior is similar to

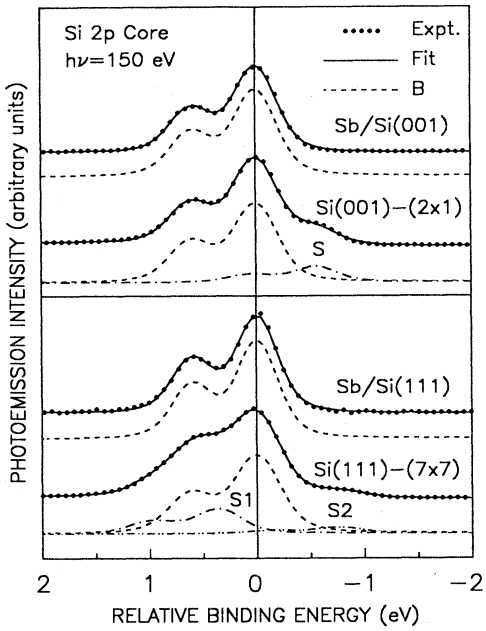

FIG. 1. Si 2*p* core-level spectra taken with a photon energy of 150 eV for the Si(111)-(7×7), Si(001)-(2×1), and Sb-saturated surfaces. The solid curves running through the data points (dots) are fits to the data. The other curves show the decomposition into bulk (*B*) and surface (*S*, *S*1, and *S*2) contributions. The binding energy is referred to the bulk Si $2p_{3/2}$ components.

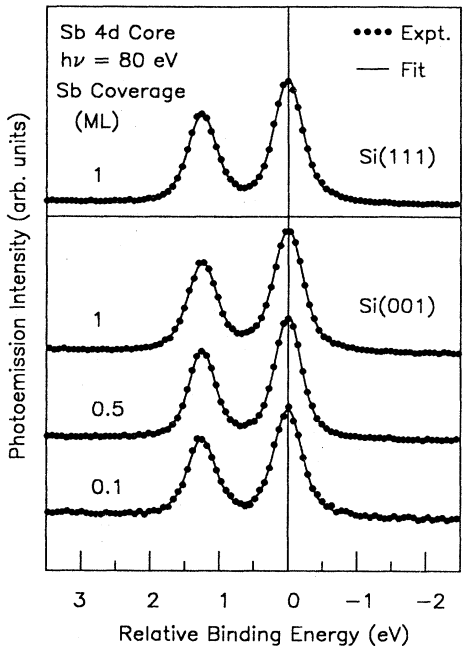

FIG. 2. Sb 4*d* core-level spectra for the Sb-covered Si(111) and Si(001) spectra. The various Sb coverages are indicated. The dots are the data, while the overall fit to the line shape is indicated by the curves. The binding energy is referred to the Sb $4d_{5/2}$ core-level component.

other covalently bonded adsorbate systems such as In/Si(001),[15] Sn/Si(001),[17] and Ge/Si(111).[14]

A few typical Sb 4*d* core-level spectra are shown in Fig. 2, and are found to consist of only one resolved spin-orbit-split component, whose width remains constant during the Sb growth for all exposures up to and including saturation for both the Si(001) and Si(111) surfaces. The solid curves are the results of a one-component fit; the fitting procedure is similar to that used for the Si 2*p* core level. The existence of only one component suggests that nearly all the Sb resides on the surface with a fair degree of chemical equivalence. The solubility of Sb in Si is less than 0.1% (5×10^{19} cm^{-3}) for this temperature range,[18] and therefore Sb incorporation into the bulk is not expected to induce a measurable effect in the Sb 4*d* core-level line shape.

Previous studies using modulated-beam mass-spectrometry techniques have shown that the sticking coefficient of Sb on Si approaches zero after the completion of the first chemisorbed Sb layer for the present substrate temperature range.[11] To illustrate this saturation behavior, the measured Sb 4*d* core-level intensity as a function of Sb exposure on Si(001) is shown in Fig. 3. The intensity is seen to saturate for Sb exposures greater than about 1 ML, implying that the accumulation of Sb on the surface is greatly reduced beyond this exposure. Similar results have been reported before for Sb on Si(111) and As on Si(111) and Si(001).[12,19]

The dots in Fig. 3 indicate the Fermi-level position relative to the band gap for Sb/Si(001) as a function of Sb exposure, which has been determined by measuring changes in the bulk Si 2*p* core-level binding energy. The Fermi level for Si(001), initially at 0.58±0.05 eV above the valence-band maximum (VBM) for the clean (2×1) surface,[19] gradually moves upward and reaches 1.21±0.12 eV above the VBM at saturation, as shown in

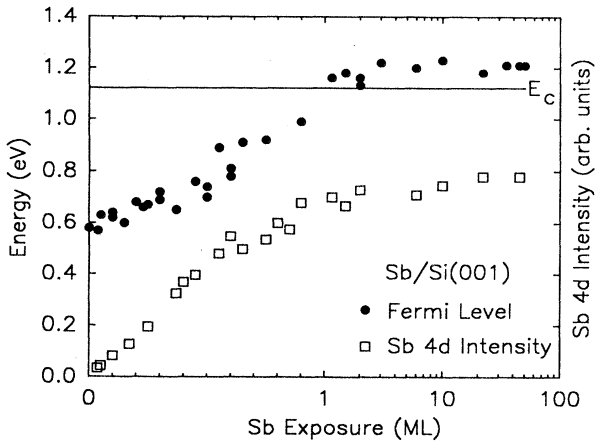

FIG. 3. Sb 4*d* core-level intensity (squares) and Fermi-level position (dots) as a function of Sb exposure. The intensity scale indicated on the right is linear. The energy scale indicated on the left is referred to the VBM. The CBM is located at 1.12 eV above the VBM and is labeled E_C. The abscissa scale is linear for Sb exposures less than 1 ML and logarithmic for exposures greater than 1 ML.

Fig. 1. Since the Si band gap is 1.12 eV, the Fermi level for saturation coverage is thus very close to or above the CBM. For Sb/Si(111) the Fermi level relative to the gap shows a very similar behavior (data not shown), and its final position at saturation coverage is the same as that for the Sb/Si(001) case. As will be shown below, these results agree with the valence-band measurements.

B. Medium-energy CBM-state resonance for Sb/Si(001)

The normal-emission spectra for the Sb-saturated Si(001) surface in the valence-band region are shown in Fig. 4 for various photon energies. Only a limited region of the valence band is shown, so that the emission occurring near the Fermi level can be emphasized. The most striking feature in Fig. 4 is the distinct sharp peak located just below the Fermi level, indicating the presence of a metallic state. This metallic peak is followed by a gap with no emission. The onset of emission below the gap is at 1.21 ± 0.05 eV binding energy with respect to the Fermi level for each spectrum shown in Fig. 4. This must then be the position of the VBM, in agreement with the core-level results shown in Fig. 3, and a dashed line labeled E_V is shown in Fig. 4 to indicate this position.

The metallic state was observed only after the Fermi level was pushed up slightly above the CBM (see Fig. 3), which only occurred at saturation coverages. The surface after saturation coverage also becomes extremely insensitive to residual-gas contamination. These observations suggest that this metallic state is not a surface state of the usual kind. The most straightforward interpretation is degenerate doping of the near-surface region, resulting in a significant population of conduction electrons near the CBM (the $\Delta_1^{\min}$ point in k space); these electrons give rise to the sharp peak in Fig. 4. The shape of the surfaces of constant energy near the Si CBM are ellipsoids of revolution centered on the Δ line away from the X point; in the event of degenerate doping, the Fermi surface will form a small ellipsoid centered about the CBM.

To verify the assertion of degenerate doping, we have determined the wave vector $\mathbf{k}$ of these electrons, which should be at $\Delta_1^{\min}$ according to our model. For all photon energies used, a slight departure from the normal-emission direction ($\sim 3°$) caused the peak to disappear, meaning that the wave-vector component parallel to the surface is zero. Figure 5 illustrates this by showing the sudden evanescence of the metallic state for small angular deviations θ from the normal direction with $\mathbf{k}_{\parallel}\|[110]$ and $h\nu=37.1$ eV. A small dispersion of the metallic-state position towards the Fermi level for increasing θ is observed just before its disappearance; this is consistent with the sign of the transverse effective mass of Si at the CBM. Since the observed angular spread of the metallic state is about the same as the acceptance angle of the analyzer, it is impossible to determine accurately this effective mass from the present data.

To determine $k_{\perp}$, the wave-vector component perpendicular to the surface, we use the well-known "$k_{\perp}$-scan" technique by plotting the normalized intensity of this peak as a function of the photon energy.[5–7] Since the relevant final band is well approximated by a broadened free-electron dispersion, the photon energy used can be directly converted to the final electron wave vector k_f by the formula

$$E_i+h\nu=\hbar^2k_f^2/2m^*-U\ , \tag{1}$$

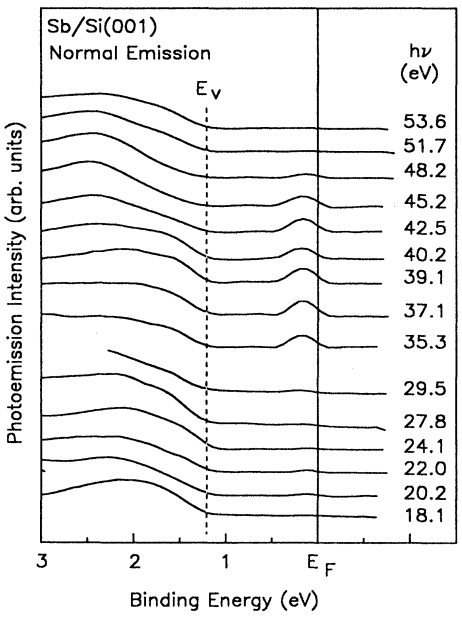

FIG. 4. Normal-emission spectra of the Sb-saturated Si(001) system for various photon energies showing the low- and medium-energy resonances centered at about 22 and 40 eV, respectively. The binding energy is referred to the Fermi level E_F and the valence-band maximum of Si is labeled E_V.

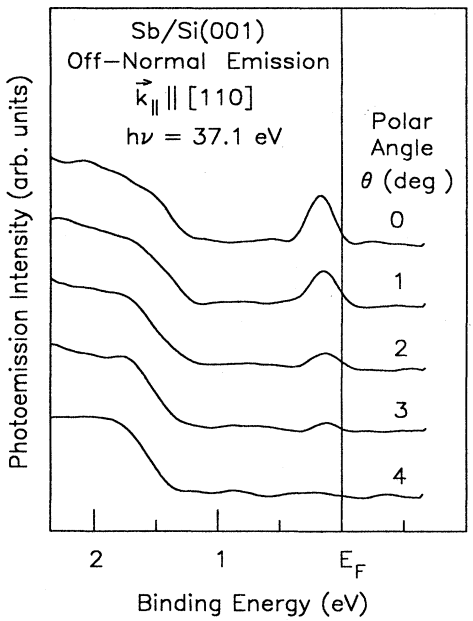

FIG. 5. Spectra of the Sb-saturated Si(001) system for small angular deviations θ from the normal direction. The photon energy is $h\nu=37.1$ eV and the direction of the component of the momenta parallel to the surface is along [110]. The binding energy is referred to the Fermi level E_F.

where E_i (the CBM state energy) and U (the inner potential) are both referred to the VBM, and m^* is the electron effective mass, which is taken to be the free-electron mass m for this photon-energy range.[5–7] The results are shown in the lower panel of Fig. 6 with U taken to be 5.6 eV (see below). This value of U is consistent with that ($\sim$5 eV) determined previously.[8,20] The intensity of the metallic state shown in Fig. 6 was normalized according to the integrated intensity of the valence-band region; the data uncertainty is dominated by the limited experimental precision, which is $\sim$10% near the peak and follows from the degree of data scattering. The results show a strong resonance centered about $k_f = 3k_{\Gamma X}$ in the extended-zone scheme ($k_{\Gamma X} = 2\pi/a = 1.16$ Å^{-1} is the distance between the Γ and X points in the Brillouin zone; a is the lattice constant of Si). The small dip near the peak of the resonance suggests the presence of two nearby peaks. To further verify the existence of the small dip, we have used the CIDS technique described in Sec. II. The raw data without correction for monochromator efficiency are shown over a narrow photon-energy range in Fig. 7. The lower and upper abscissa show the photon energy and k_f, respectively. Indeed, a dip in the CBM-state intensity is observed for $k_f = 3k_{\Gamma X}$, in agreement with the results of Fig. 6. Shown in the upper panel in Fig. 6 are the dispersion curves for the highest valence band and the lowest conduction band of Si taken from the calculation of Chelikowsky and Cohen,[21] presented in the repeated-zone scheme. The energy zero for the ordinate is the VBM. The two nearby resonance peaks, indicated by the vertical dashed lines, correspond very well with the CBM, which is located very near, but not at, the X critical point. This is strong evidence that our interpretation is correct.

Within the direct-transition model the position and linewidth of the resonance are determined by the value of k_i, the initial electron wave vector, and by broadening effects, respectively.[5–7] The solid curve describing the data in Fig. 6 is a least-squares fit based on this model. The model function is a superposition of two Voigt functions (convolution of a Gaussian and a Lorentzian) as indicated near the bottom of Fig. 6, each separated from the X critical point by an adjustable amount (same for both components). The inner potential was also made adjustable in the fit; the final value was 5.6 eV (see above). From the fit, the centers of the two Voigt line shapes occur at $k_i = (3 \pm 0.09)k_{\Gamma X}$, meaning that the CBM, or the $\Delta_1^{\min}$ point, is separated from the Brillouin-zone center Γ by $0.91k_{\Gamma X}$. This is very close to Chelikowsky's and Cohen's theoretical result of $0.89k_{\Gamma X}$,[21] and differs somewhat from Feher's result of $0.85k_{\Gamma X}$ deduced from a model fitted to the electron-spin-resonance data.[22] The Lorentzian width of the Voigt functions represents the

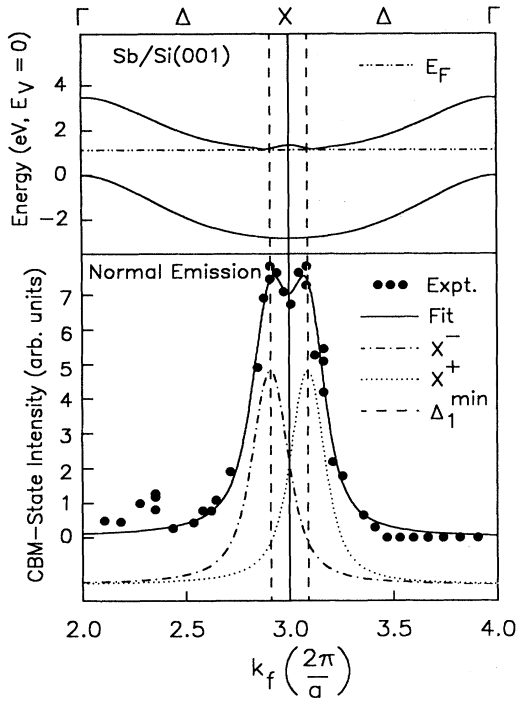

FIG. 6. Lower panel shows the CBM-state intensity as a function of k_f (measured in units of $2\pi/a$), which is determined from Eq. (1). The data (dots), the fit to the data (solid curve), the individual X^- and X^+ components (dashed-dotted and dotted curves), and the resulting $\Delta_1^{\min}$ positions (dashed vertical lines) are indicated. The data uncertainty is dominated by the limited experimental precision in the intensity measurement, which is less than about 10% near the peak and follows from the degree of data scattering. The upper panel shows the highest valence band and the lowest conduction band along the Δ line (from Ref. 21), with the initial energy referred to the VBM at E_V. The Sb-induced Fermi-level position (E_F) is indicated.

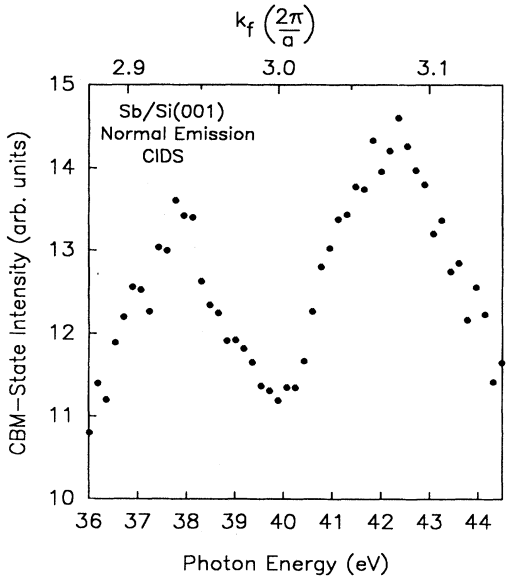

FIG. 7. Constant-initial-state–difference spectroscopy (CIDS) measurements for the medium-energy CBM-state resonance near $k_i = 3k_{\Gamma X}$. The lower and upper abscissa show, respectively, the photon energy and the final-state momenta based on Eq. (1) using $m^* = m$. The dip in the CIDS intensity near 40 eV confirms the results of Fig. 6 near $k_f = 3k_{\Gamma X}$.

final-state electron lifetime broadening; from the fit, a value of 4.3 eV is obtained, which translates into a 6.2-Å mean free path using the free-electron group velocity at $k_f = 3k_{\Gamma X}$. This value is consistent with the mean free path in Si obtained from core-level spectroscopy.[23] The Gaussian width represents the distortion and smearing of the free-electron final-state character; the fit gives a value of 3.4 eV, which is close to the expected values based on the typical order of pseudopotential form factors (~ 3 eV).[5,6,21] Thus, all of the essential features of the medium-energy-resonance behavior are nicely explained.

C. Low-energy CBM-state resonance for Sb/Si(001)

The spectra in Fig. 4 and the cross section shown in Fig. 6 indicate the existence of a weaker resonance near $h\nu = 22$ eV. The results from a CIDS scan are shown in Fig. 8. An even weaker resonance can also be seen at $h\nu = 19$ eV. Since the model of a free-electron-like final band is a good approximation only at high energies, the analysis described above for the medium-energy resonance is not expected to be applicable for such low photon energies.[5–8] Indeed, a straightforward application of the above model using Eq. (1) shows that the medium-energy resonance is the lowest resonance. Since the actual final band structure of Si at ~ 20 eV above the Fermi level is rather complex and not well known, we have not attempted a detailed analysis for these low-energy resonances.

Figure 9 shows off-normal scans of the resonance with $h\nu = 22$ eV. Again, the CBM peak is seen to rapidly decrease with increasing angular deviations θ from the normal direction with $\mathbf{k}_\parallel \| [110]$. This result is consistent with the suggestion that the low-energy resonances are due to direct transitions to some unspecified final bands, so $\mathbf{k}_\parallel$ remains zero.

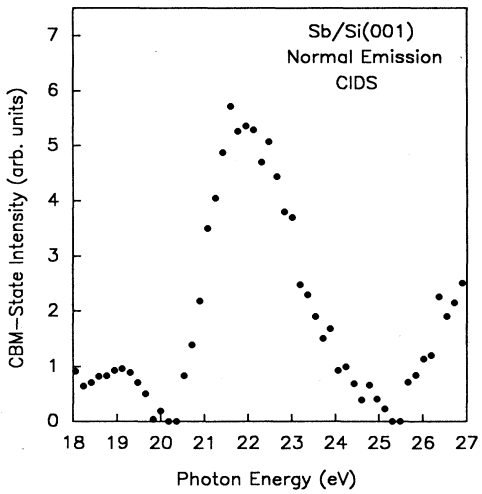

FIG. 8. Constant-initial-state–difference spectroscopy measurements for the low-energy CBM-state resonance near $h\nu \approx 22$ eV. The photon energy is indicated on the abscissa.

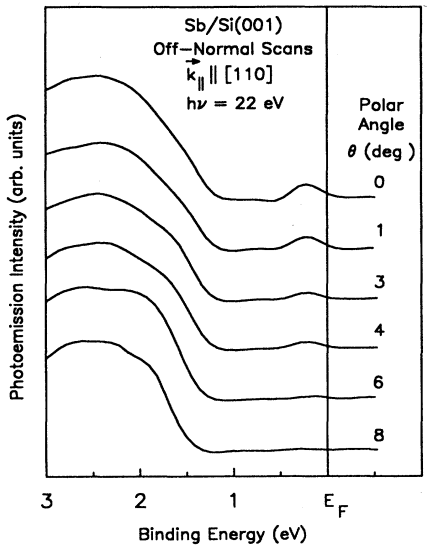

FIG. 9. Spectra of the Sb-saturated Si(001) system for small angular deviations θ from the normal direction. The photon energy is 22 eV and the direction of the component of the momenta parallel to the surface is along [110]. The binding energy is referred to the Fermi level E_F.

D. High-energy CBM-state resonance for Sb/Si(001)

Owing to the periodicity of the band structure, multiple CBM-state resonances should be observed in the normal-emission geometry for $k_f = (2n + 1 \pm 0.09)k_{\Gamma X}$ for integer n. The case of $n = 1$ corresponds to the medium-energy resonance discussed above. We have searched for the next resonance at $n = 2$; some of the spectra are shown in Fig. 10 for $98 \leq h\nu \leq 118$ eV. A distinct CBM-state resonance is found to be centered about $h\nu = 106$ eV. The measurement is distorted for $100 \lesssim h\nu \lesssim 101$ eV due to Si $2p$ core-level emission excited by stray second-order light from the monochromator; this second-order peak can be clearly seen in the 99-eV spectrum just above the VBM. Apart from this minor complication, the results are similar to those shown in Fig. 4 for the medium-energy resonance. The metallic state in each spectrum is followed by a gap with no emission, and the onset of emission below the gap is at 1.21 ± 0.05 eV binding energy with respect to the Fermi level. Using CIDS, the intensity behavior has been analyzed, and the raw data are shown in Fig. 11. A somewhat asymmetric peak is seen at $h\nu \approx 106$ eV.

From Eq. (1), the predicted center of the resonance for $k_f = 5k_{\Gamma X}$ using the free-electron mass for m^* is at $h\nu = 122$ eV, but the only resonance that we found near this region is that at ~ 106 eV. It is apparent that a modification must be made to the model. Depending on the theoretical concepts, either the inner potential or the effective mass could be taken to be energy dependent. In the simplest interpretation, the inner potential is the average electrostatic potential within the solid (Hartree approximation) and is energy independent; all many-body corrections beyond the Hartree approximation are modeled by an energy-dependent effective mass. A sim-

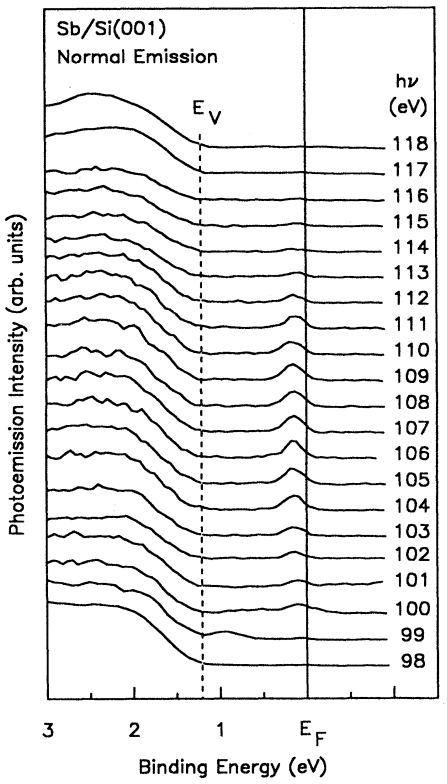

FIG. 10. Normal-emission spectra of the Sb-saturated Si(001) system for various photon energies showing the high-energy resonance centered about 106 eV. The binding energy is referred to the Fermi level E_F and the valence-band maximum of Sb-saturated surface is labeled E_V.

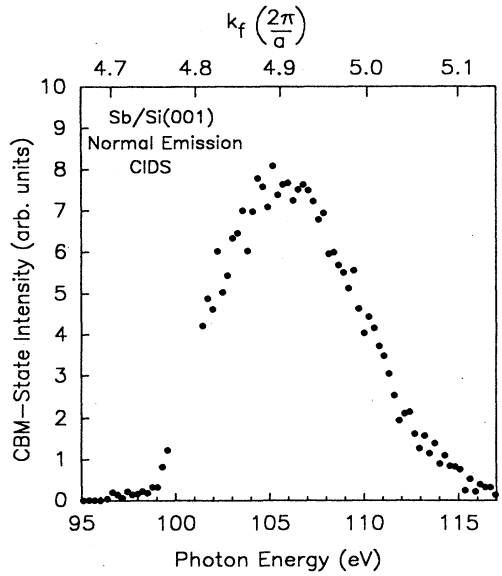

FIG. 11. Constant-initial-state–difference spectroscopy measurements for the high-energy CBM-state resonance. The photon energy and the final-state momenta calculated from Eq. (1) using $m^*=1.10m$ are shown on the lower and upper abscissa of the figure, respectively.

ple example of many-body corrections is the interaction with the core electrons. The motion of the hot electron depends upon whether or not the energy of the hot electron is sufficient to excite the core electrons to the conduction band. Likewise, the scattering by plasmons depends on energy and contributes to the energy dependence of the hot-electron effective mass. Free-electron-like final-state models which incorporate an energy-dependent effective mass have been used for photoemission of various noble-metal surfaces.[24,25]

If we assume the peak center at $h\nu=106$ eV in Fig. 11 corresponds to $k_f=5k_{\Gamma X}$, then Eq. (1) yields $m^*/m=1.14$ and the photon energies corresponding to the $k_f=(5\pm0.09)k_{\Gamma X}$ transitions at $\Delta_1^{\min}$ are 102 and 110 eV. An attempt to fit this line shape based on the same procedure described above for the medium-energy resonance was unsuccessful; clearly, the line shape of Fig. 11 is too narrow to account for two peaks separated by 8 eV. In comparing the energy width between the medium- and high-energy resonances, the final-state lifetime broadening should approximately scale with the group velocity since the mean free path is not expected to change significantly between $h\nu=40$ and 106 eV.[23] Therefore, the energy width of each $\Delta_1^{\min}$ peak is expected to be broadened in approximate proportion to the energy separation between them, and with our model two peaks should be observable. Therefore, it is apparent that the sharp peak occurring at 106 eV cannot be caused by transitions from both $k_f=(5\pm0.09)k_{\Gamma X}$ resonances, and we adopt the interpretation that only one of the resonances causes the main intensity peak. A small asymmetric tail is observed towards higher photon energies (112–115 eV) relative to the lower-photon-energy side of the peak, and this may be due to the second transition. We admit that this tentative interpretation is speculative at this stage (for example, why are the intensities of the two resonances so different?), but this is the best we can offer. Additional supporting evidence for this assignment derived from bulk band measurements will be presented below. Using Eq. (1), with $k_f=4.91k_{\Gamma X}$ for the peak at $h\nu=106$ eV, we obtain $m^*/m=1.10$, and the upper abscissa of Fig. 11 for k_f is based on this effective-mass value. A similar increase in effective mass value is observed for the mapping of the final-state band dispersion of Ag(111), where it is found that $m^*/m=1.08$ for final states $\sim$150 eV above the Fermi level.[25]

In order to verify that the full wave vector **k** corresponds to emission from $\Delta_1^{\min}$, we have performed the usual off-normal measurements, which are shown in Fig. 12. The sudden evanescence of the metallic state for small angular deviations θ indicates that $k_\parallel=0$. The barely detectable dispersion of the state towards the Fermi level is, again, consistent with the sign of the transverse effective mass of Si at the CBM.

E. Degenerate doping for Sb/Si(110) and Sb/Si(111)

By examining the onset of emission of the valence-band region for the Sb-saturated Si(110) and Si(111) surfaces in the normal-emission spectra, the position of the Fermi level is found to lie $\sim$1.2 eV above the VBM. For

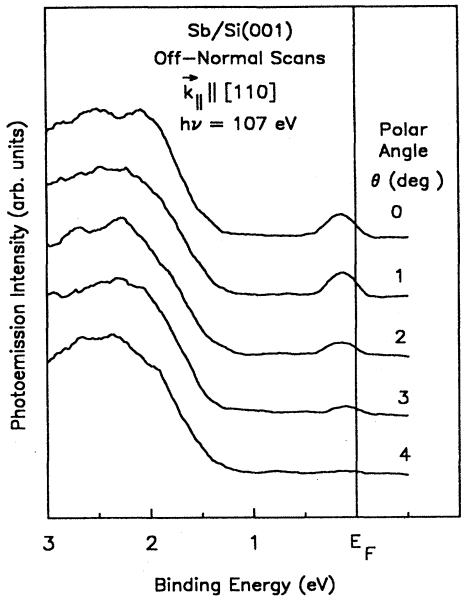

FIG. 12. Spectra of the Sb-saturated Si(001) system for small angular deviations θ from the normal direction. The photon energy is 107 eV and the direction of the component of the momenta parallel to the surface is along [110]. The binding energy is referred to the Fermi level E_F.

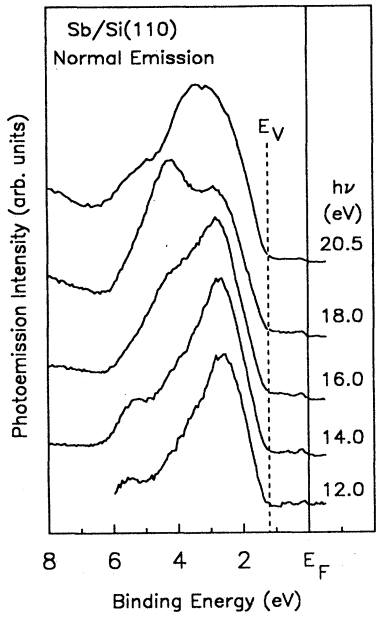

FIG. 13. Normal-emission spectra of the Sb-saturated Si(110) system for various photon energies. The binding energy is referred to the Fermi level E_F and the valence-band maximum is labeled E_V.

Sb/Si(111) this corroborates the Si $2p$ core-level measurements. The Sb-saturated Si(110) normal-emission spectra are shown in Fig. 13 for various photon energies. The position of the VBM is indicated with a dashed line and is labeled E_V. A very small peak is observed just below the Fermi level for each spectrum in Fig. 13, similar to what has been observed for Sb/Si(001). The X critical point can be reached by normal emission from Si(110), which samples momenta along the Γ-K-X direction of the bulk Brillouin zone. While the $\Delta_1^{\min}$ points are off normal in this geometry, final-state broadening and the limited angular resolution is expected to enable the detection of the CBM state. For these low photon energies, however, the final-state band dispersion is uncertain, and we have not attempted to determine the **k** value for the initial state since a full determination has already been done for the Sb/Si(100) system. The Sb/Si(111) normal-emission spectra of the Fermi-level region (not shown here) do not show a metallic peak from the CBM state, even though the VBM is at $\sim$1.2 eV below the Fermi level. This is understandable, as the normal-emission geometry does not allow the detection of direct transitions from the CBM for this surface orientation.

F. Discussion of doping mechanisms

By comparing the integrated intensity of the CBM state for Sb/Si(001) at resonance over its narrow cone of emission of the integrated intensity of the valence-band region summed over all angles due to the four valence electrons per Si atom, we estimate a carrier concentration of 10^{19}–10^{20} electrons/cm^3 in the conduction band within the photoemission probing depth of $\sim$6 Å. This is close to the expected doping concentration necessary to raise the Fermi level into the conduction band.[26] Zeindl *et al.*,[1] using Hall measurements, have shown that a Sb-dopant concentration of $\sim 10^{20}$ cm^{-3} in Si can cause metallic conductivity. Since the spatial confinement of the donor electronic charge is on the order of the Sb-donor radius of 20 Å,[27] which is greater than the photoemission probing depth, a dense Sb-doping profile near the surface is sufficient to cause the degenerate-doping conditions observed here. The modification in electronic properties beyond the photoemission probing depth caused by this Sb-saturation method depends on the details of the Sb-solubility and bulk-diffusion phenomena, which cannot be determined from our data. The concentration of donors can significantly be enhanced by ion-implantation techniques, although this tends to degrade the structural quality of the crystal compared to MBE methods. In another study, Eastman *et al.*,[28] using a constant photon energy of 21 eV and an off-normal emission geometry, have shown that an As-implanted Si(111)-(1×1) surface may exhibit a metallic emission due to an initial-state occupation at the CBM. However, the electron momentum is uncertain in this study since the final-state band dispersion is unknown for this photon energy.

The fact that degenerate doping is achieved only after saturation coverage on the surface can be explained in a couple of ways. In Fig. 3 it is evident that for a coverage of 0.5 ML the Fermi level is still $\sim$0.4 eV below the CBM. In a recent STM and core-level study of Sb/Si(001) it was observed that at $\sim$0.5-ML coverage the

Si $2p$ core-level spectrum exhibits no contribution from dimer atoms, and all dangling bonds are saturated.[13] This observation is important in connection with the mechanisms which are believed to pin the Fermi level on the clean Si(001)-(2×1) surface.[29,30] If one believes that there is substantial empty surface density of states within the gap due to the Si surface dangling bonds,[29,30] then saturation of all surface dangling bonds should eliminate the surface density of states within the gap which can pin the Fermi level. The fact that an additional ~0.5 ML of Sb is needed after the elimination of the dangling bonds to move the Fermi level into the CBM points to other mechanisms which may pin the Fermi level. Recently, Hamers and Kohler have shown that certain defects may play a role in Fermi-level pinning.[30] Thus, further Sb coverage after removal of the dangling bonds may be needed to suppress defect-related states. In any event, the behavior of the Fermi level with coverage in Fig. 3 suggests that the removal of the pinning mechanism is gradual up to the saturation coverage.

An alternative explanation, and one not incompatible with the above interpretation, is that the degenerate doping is actually due to Sb incorporation into the bulk lattice. It is possible that significant bulk incorporation, limited by bulk solubility, can occur only after all surface sites are occupied. This is related to the question of bulk diffusion versus surface segregation. The present results cannot influence a decision on these possibilities. Experimentally, it appears, however, that the degenerate-doping condition is only a function of total coverage, independent of annealing time and small variations in annealing temperature (too high a temperature causes the Sb to desorb, and too low a temperature causes bulk accumulation of Sb on the surface). Thus, bulk diffusion probably does not play an important role in the degenerate doping. If we assume that essentially all of the active donors are confined to the surface, then we can estimate the total carrier density per unit surface area to be the product of the donor charge radius (~20 Å) and the carrier density near the surface (10^{19}–10^{20} cm^{-3}). The result is between 2×10^{12} and 2×10^{13} cm^{-2} (or $\frac{1}{300}$–$\frac{1}{30}$ ML). This level of active Sb donors out of 1 ML total Sb coverage can be easily explained by the presence of defects, steps, and other minority sites at the surface.[13,30]

G. Sb-induced bulk band transitions in Si(001) and Si(111)

The effect of the Sb passivation of Si(001) and Si(111) on bulk valence-band transitions and surface states has been investigated. The angle-resolved normal-emission spectra for the clean Si(111)-(7×7) and Si(001)-(2×1) surfaces are shown at the bottoms of Figs. 14 and 15, respectively, and are consistent with previous measurements.[8,31,32] The surface states in the Si(111)-(7×7) spectrum are labeled $T1$, $T2$, and $T3$, and have been previously identified from STM as being derived from the adatam dangling bonds, rest-atom dangling bonds, and adatom backbonds, respectively.[14,33] The Si(001)-(2×1) spectrum contains a strong surface-state feature labeled T, and STM shows that it originates from the dimer dangling bonds.[34] At Sb saturation the dangling-bond states are no longer present. This is consistent with the core-level and STM findings, which indicate that all Si-surface dangling bonds are saturated by Sb absorption.

The normal-emission spectra for Sb-saturated Si(111) are shown in Fig. 14, and the spectra for Sb-saturated Si(001) are shown in Figs. 15–17. Several nondispersive emission features are apparent. These peaks may be derived from critical points associated with the one-dimensional density-of-states features, from three-dimensional density-of-states features, or from Sb-induced surface or interface states. Their assignment based on the present experiment is uncertain, and the emphasis here will be on the dispersive features, labeled $A1$, $B1$, $C1$, $A2$, $B2$, $C2$, $D2$, $A3$, $B3$, and $C3$ in Figs. 14–17. Peaks $B1$ and $B2$ have a nearly constant kinetic energy and are derived from the Sb NVV Auger transition. In Fig. 16 the data for $102 \lesssim h\nu \lesssim 112$ eV showed a large hump having nearly constant kinetic energy due to the Si LVV Auger transition, and this feature has been removed from the spectra for the sake of clarity. The other dispersive peaks can be identified as direct transitions from the bulk Si valence bands; only peaks $C2$ and $D2$ have been previously observed for the case of clean Si(001)-(2×1).[8]

The technique of $k_\perp$ band mapping has been discussed in detail for the GaAs and Ge surfaces,[5–7] and the assignment of the present dispersive peaks are facilitated by

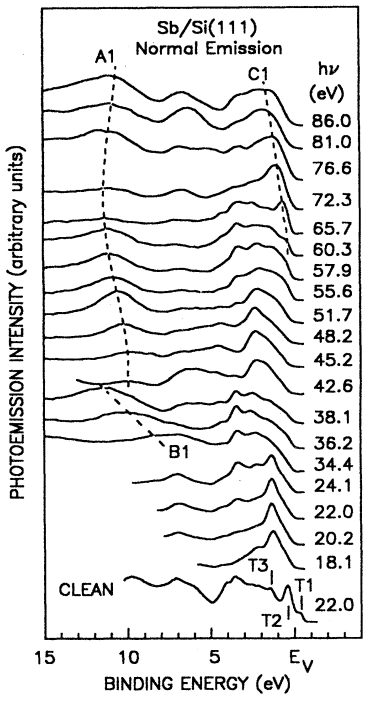

FIG. 14. Normal-emission spectra for the Si(111)-(7×7) and Sb-saturated Si(111) surfaces taken with various photon energies. The binding energy is referred to the valence-band maximum (E_V). Dispersive peaks are indicated by the dashed curves and labeled for clarity. The clean Si(111)-(7×7) spectrum is shown at the bottom for $h\nu=22.0$ eV; various surface states are indicated by the labels $T1$, $T2$, and $T3$.

comparison with these studies. The formalism is the same which has been employed for the CBM state in Sb/Si(001). The theoretical valence-band dispersions of Si along the Γ-Δ-X and Γ-Λ-L directions obtained by Chelikowsky and Cohen using a local pseudopotential (dashed curve) and a nonlocal pseudopotential (solid curve) method are shown in Fig. 18. Peaks $C1$, $C2$, and $B3$ are assigned as direct transitions from the uppermost valence band, while peaks $A1$, $A2$, $A3$, and $C3$ are assigned as direct transitions from the lower valence bands. Transition $A3$, the s-like band for $h\nu \lesssim 120$ eV, gradually evolves into $C3$, the middle valence band for $h\nu \gtrsim 120$ eV.

The final band used for band mapping is described by Eq. (1). For both Sb/Si(111) and Sb/Si(001) systems we have used a final-state effective mass $m^* = m$ for $h\nu \leq 86$ eV, which corresponds to the same effective mass used for the medium-energy CBM-state resonance of Sb/Si(001). For higher photon energies ($h\nu \geq 92$ eV), we have used $m^* = 1.10m$, which is the effective mass used for the high-energy CBM-state resonance. The same inner potential of 5.6 eV is used for all energies. The peak $D2$ corresponds to a final-state energy too low to be approximated by the free-electron dispersion as discussed previously,[8] so it is not analyzed here. The resulting band dispersions from Sb/Si(111) are indicated in Fig. 18 by solid circles, and diamonds and squares are used to indicate the band dispersions for Sb/Si(001) for $h\nu \geq 92$ eV and $h\nu \leq 81$ eV, respectively. The typical energy error shown in Fig. 18 reflects the uncertainty in peak-position determination; the typical momentum error is mainly due to the uncertainty in the inner potential, effective mass, and the broadening of the free-electron final band by crystal-potential and lifetime effects. Allowing for errors, the agreement between experiment and theory is generally good. The experimental determination of the X_1 and X_4 critical points (-9.0 and -3.3 eV with respect to the VBM, respectively) is in agreement between the low- and high-photon-energy transitions; this further adds credence to our effective-mass assignment for the final-state band. If the other choice of $m^* = 1.14m$ were used, which would place the center of the high-energy CBM-state resonance ($h\nu = 106$ eV in Fig. 11) at $k_i = 5k_{\Gamma X}$, the resulting X_1 critical point would be too low (-9.8 eV with respect to the VBM), and the overall agreement with the theoretical calculations would be much worse. Also note that in Fig. 16 peak $B3$ evolves into a nondispersive peak at about $h\nu = 114$ eV. This is a fairly typical behavior observed in band mapping and is associated with reaching a critical point (X_4) on the zone boundary.[5-8] Subtracting the binding energy of 3.3 eV of X_4 from the photon energy $h\nu = 114$ eV yields ~ 111 eV above the VBM for the final band at the X point. This agrees with Eq. (1) for $m^* = 1.10m$ and $E_i = 0$, which further sup-

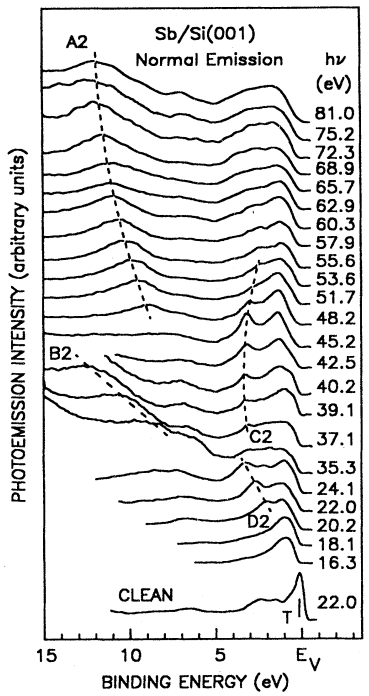

FIG. 15. Normal-emission spectra for the Si(001)-(2×1) and Sb-saturated Si(001) surfaces taken with the indicated photon energies. The binding energy is referred to the valence-band maximum (E_V). Dispersive peaks are indicated by the dashed curves and labeled for clarity. The clean Si(001)-(2×1) spectrum is shown at the bottom for $h\nu = 22.0$ eV; the surface state is indicated by the label T.

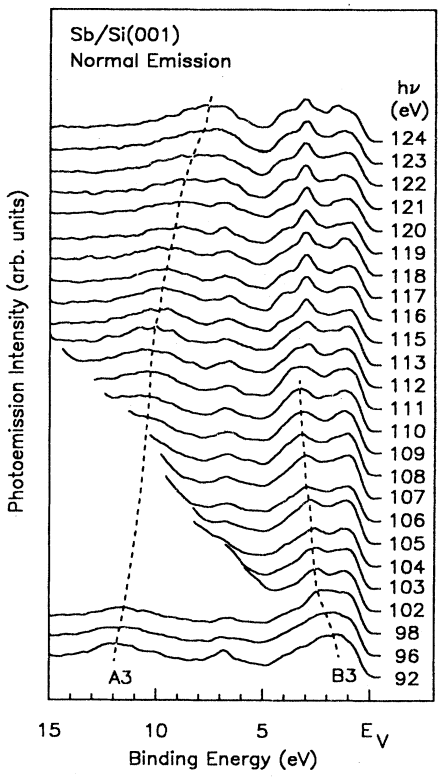

FIG. 16. Normal-emission spectra of the Sb-saturated Si(001) surface for $92 \leq h\nu \leq 124$ eV. The binding energy is referred to the valence-band maximum (E_V). Dispersive peaks are indicated by dashed curves and labeled for clarity.

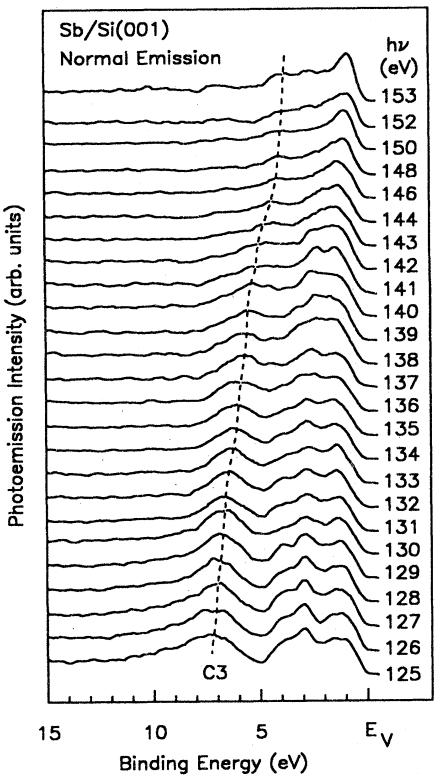

FIG. 17. Normal-emission spectra of the Sb-saturated Si(001) surface for $125 \leq h\nu \leq 153$ eV. The binding energy is referred to the valence-band maximum (E_V). Dispersive peaks are indicated by dashed curves and labeled for clarity.

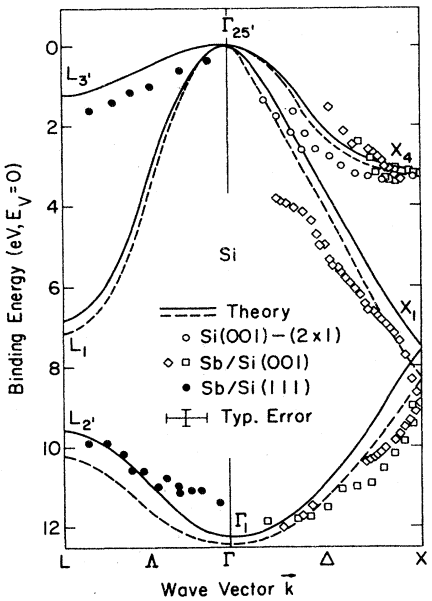

FIG. 18. Bulk valence-band structure of Si along the Γ-Λ-L and Γ-Δ-X directions. The solid and dashed curves are theoretical calculations from a nonlocal and local pseudopotential method, respectively, from Ref. 21. The open circles are from Ref. 8. The solid circles are data obtained from bulk band dispersions on Sb-saturated Si(111). The squares and diamonds are data obtained from band dispersions on Sb-saturated Si(001) for $37.1 \leq h\nu \leq 81$ and $92 \leq h\nu \leq 153$ eV, respectively.

ports our choice of the effective mass.

The absence of dispersive bulk band transitions from the clean Si(111)-(7×7) and Si(001)-(2×1) systems under similar experimental conditions was speculated to be caused by surface strain and reconstruction, and the resulting crystal-lattice distortion was argued to extend at least on the order of the photoelectron escape depth of Si (5–7 Å).[8] Since the Sb termination is found to suppress the reconstructions and to saturate all surface dangling bonds, leading to a bulklike chemical environment, the Sb-induced bulk band transitions observed here are possibly due to a reduction in lattice distortion caused by adsorbate-to-substrate bonding. There exists other evidence in the literature that adsorbates can modify the surface strain. Uhrberg, Bringans, Olmstead, and Bachrach, using a constant photon energy of 21.2 eV and off-normal scans, demonstrated that the As termination of Si(111) sharpens certain peaks in the valence-band spectra.[35] Low-energy electron-diffraction results also show that adsorbates can reduce the surface relaxation for a variety of metal surfaces.[36]

IV. SUMMARY AND CONCLUSIONS

We have presented extensive photoemission results for the Sb-saturated Si(001) surface, and to a lesser degree, for the Sb/Si(111) and Sb/Si(110) systems. The photoemission results indicate clearly that the Fermi level crosses the CBM of Si for all three systems. A distinct metallic peak within a narrow energy and momentum window is observed for Sb/Si(001), and distinct resonances are observed which show characteristics features of direct transitions from the $\Delta_1^{\min}$ points (CBM) to different final states. For the medium energy resonance located near $k_i = 3k_{\Gamma X}$, the resonance is fitted well with a model function which incorporates the inner potential, $\Delta_1^{\min}$ position, and final-state electron lifetime- and crystal-potential-broadening effects. CIDS has been employed to more accurately measure small changes in the CBM-state intensity resonance. The high-energy resonance near $k_i = 5k_{\Gamma X}$ suggests an increase in the electron effective mass for the final band. A small metallic-state emission from the CBM is also seen in the normal-emission spectra for Sb/Si(110). The present experiment demonstrates that the combination of $k_\perp$ and $k_\parallel$ scans yields a full determination of the k-space location of the conduction-band minimum of Si, and represents an interesting application of angle-resolved photoemission spectroscopy to explore conduction-band properties. The results further reveal that under conventional MBE conditions the Si surfaces can be degenerately doped by saturation coverage of Sb. The present findings are particularly relevant in view of the current interest in the metallization of semiconductor surfaces and fabrication of high-quality Ohmic contacts used to enhance device performance. Even though degenerate doping can also be achieved though ion implantation, this technique does not allow for the high-quality crystalline and electronic characteristics obtained from the MBE procedure.

The core-level measurements reveal that the Sb termination of Si(001) and Si(111) causes the Si surface

atoms to reside in a bulklike atomic environment. Angle-resolved studies of the valence-band region over a wide photon-energy range can show the presence of dispersive peaks which were previously unobserved for the clean Si(111)-(7×7) and Si(001)-(2×1) surfaces. These results strongly suggest that the Sb termination causes a reduction in strain for the outermost Si layers on Si(111) and Si(001). The bulk band dispersions have been mapped along the Γ-Λ-L and Γ-Δ-X high-symmetry directions and are compared with the theoretical calculations of Chelikowsky and Cohen. The inner potential and electron effective mass for the final band obtained from a model fitted to the medium-energy CBM-state resonance is seen to yield experimental valence-band dispersions for the Sb-saturated Si(111) and Si(001) surfaces consistent with the theory. At higher energies it is found to be necessary to adjust the effective mass to account for the energies and peak evolution near the X_1 and X_4 critical points, and the adjustment is consistent with that deduced from the high-energy CBM-state resonance.

ACKNOWLEDGMENTS

This material is based upon work supported by the U.S. Department of Energy (DOE), Division of Materials Sciences, under Contract No. DE-AC02-76ER01198. Some of the personnel and equipment support was also derived from grants from the National Science Foundation (NSF) (Grants No. DMR-83-52083 and No. DMR-86-14234), the IBM Thomas J. Watson Research Center (Yorktown Heights, NY), and E. I. du Pont de Nemours and Company (Wilmington, DE). We acknowledge the use of central facilities of the Materials Research Laboratory of the University of Illinois, which was supported by the U.S. DOE, Division of Materials Sciences, under Contract No. DE-AC02-76ER01198, and the NSF under Contract No. DMR-83-16981.

*Present address: Jet Propulsion Laboratory, California Institute of Techonlogy, 4800 Oak Grove Drive, Pasadena, California 91109.

[1]H. P. Zeindl, T. Wegehaupt, I. Eisele, H. Oppolzer, H. Reisinger, G. Tempel, and F. Koch, Appl. Phys. Lett. **50**, 1164 (1987).

[2]A. Zrenner, H. Reisinger, F. Koch, and K. Ploog, in *Proceedings of the 17th International Conference on Physics of Semiconductors, San Francisco, 1984,* edited by D. J. Chadi and W. A. Harrison (Springer-Verlag, New York, 1985), p. 325.

[3]D. H. Rich, A. Samsavar, T. Miller, F. M. Leibsle, and T.-C. Chiang, Phys. Rev. B **40**, 3469 (1989).

[4]G. J. Lapeyre, J. Anderson, P. L. Gobby, J. A. Knapp, Phys. Rev. Lett. **33**, 1290 (1974).

[5]T.-C. Chiang, J. A. Knapp, M. Aono, and D. E. Eastman, Phys. Rev. B **21**, 3513 (1980).

[6]T.-C. Chiang, R. Ludeke, M. Aono, G. Landgren, F. J. Himpsel, and D. E. Eastman, Phys. Rev. B **27**, 4770 (1983).

[7]T. C. Hsieh, T. Miller, and T.-C. Chiang, Phys. Rev. B **30**, 7005 (1984).

[8]A. L. Wachs, T. Miller, T. C. Hsieh, A. P. Shapiro, and T.-C. Chiang, Phys. Rev. B **32**, 2326 (1985).

[9]D. H. Rich, T. Miller, G. E. Franklin, and T.-C. Chiang, Phys. Rev. B **39**, 1438 (1989).

[10]S. L. Hulbret, J. P. Scott, F. C. Brown, and N. Lien, Nucl. Instrum. Methods **208**, 43 (1983).

[11]S. A. Barnett, H. F. Winters, and J. E. Greene, Surf. Sci. **165**, 303 (1986).

[12]R. A. Metzger and F. G. Allen, J. Appl. Phys. **55**, 931 (1984).

[13]D. H. Rich, F. M. Leibsle, A. Samsavar, E. S. Hirschorn, T. Miller, and T.-C. Chiang, Phys. Rev. B **39**, 12 758 (1989).

[14]T. Miller, T. C. Hsieh, and T.-C. Chiang, Phys. Rev. B **33**, 6983 (1986).

[15]D. H. Rich, A. Samsavar, T. Miller, H. F. Lin, T.-C. Chiang, J.-E. Sundgren, and J. E. Greene, Phys. Rev. Lett. **58**, 579 (1987).

[16]D. H. Rich, T. Miller, and T.-C. Chiang, Phys. Rev. B **37**, 3125 (1988), and references therein.

[17]D. H. Rich, T. Miller, A. Samsavar, H. F. Lin, and T.-C. Chiang, Phys. Rev. B **37**, 10 221 (1988).

[18]F. A. Trumbore, Bell Syst. Tech. J. **39**, 205 (1960); S. M. Hu, in *Atomic Diffusion in Semiconductors,* edited by D. Shaw (Plenum, New York, 1973), Chap. 5, p. 336.

[19]R. D. Bringans, M. A. Olmstead, R. I. G. Uhrberg, and R. Z. Bachrach, Phys. Rev. B **36**, 9569 (1987); **34**, 7447 (1986).

[20]S. Y. Tong, H. Huang, C. M. Wei, W. E. Packard, F. K. Men, G. Glander, and M. B. Webb, J. Vac. Sci. Technol. A **6**, 615 (1988).

[21]J. R. Chelikowsky and M. L. Cohen, Phys. Rev. B **14**, 556 (1976).

[22]G. Feher, Phys. Rev. B **114**, 1219 (1959). The CBM was determined to be at $(0.85\pm0.03)k_{\Gamma X}$. The quoted uncertainty represents the averaged discrepancy of experiment with the theoretical model used for fitting the electron-spin-resonance data. A different k value will be obtained if a different fitting model is used, according to G. Feher. Thus, the accuracy of this result is unknown.

[23]T.-C. Chiang, CRC Crit. Rev. Solid-State Mater. Sci. **14**, 269 (1988).

[24]S. D. Kevan and R. H. Gaylord, Phys. Rev. B **36**, 5809 (1987).

[25]A. Samsavar, T. Miller, and T.-C. Chiang (unpublished).

[26]The Fermi-level position as a function of the donor concentration can be calculated from charge-neutrality conditions and Fermi statistics; see, for example, S. M. Sze, *Physics of Semiconductor Devices,* 2nd ed. (Wiley, New York, 1981), pp. 16–27. We assume the donor-level binding energy to be described by a Mott-transition behavior in which all the donors are ionized after a critical concentration of 1.7×10^{18} cm^{-3} (see Ref. 27). For donor densities $10^{19} < N_D < 10^{20}$ cm^{-3}, the Fermi level is above the CBM by $0 < E_F - E_C < 0.1$ eV.

[27]P. P. Edwards and M. J. Sienko, J. Am. Chem. Soc. **103**, 2967 (1981).

[28]D. E. Eastman, P. Heiman, F. J. Himpsel, B. Reihl, D. M. Zehner, and C. W. White, Phys. Rev. B **24**, 3647 (1981).

[29]P. Mårtensson, A. Cricenti, and G. V. Hansson, Phys. Rev. B **33**, 8855 (1986).

[30]R. J. Hamers and U. K. Kohler, J. Vac. Sci. Technol. A **7**, 2854 (1989).

[31]J. E. Demuth, B. N. J. Parsson, and A. J. Schell-Sorokin, Phys. Rev. Lett. **51**, 2214 (1983), and references therein.
[32]F. J. Himpsel and D. E. Eastman, J. Vac. Sci. Technol. **16**, 1297 (1979).
[33]R. J. Hamers, R. M. Tromp, and J. E. Demuth, Phys. Rev. Lett. **56**, 1972 (1986); Surf. Sci. **181**, 346 (1987).
[34]R. J. Hamers, Ph. Avouris, and F. Bozso, J. Vac. Sci. Technol. A **6**, 508 (1988).
[35]R. I. G. Uhrberg, R. D. Bringans, M. A. Olmstead, and R. Z. Bachrach, Phys. Rev. B **35**, 3945 (1987).
[36]A. P. Baddorf, I.-W. Lyo, E. W. Plummer, and H. L. Davis, J. Vac. Sci. Technol. A **5**, 782 (1987).